Science Advances

AAAS

advances.sciencemag.org/cgi/content/full/3/11/eaao3170/DC1

Supplementary Materials for

Stitching h-BN by atomic layer deposition of LiF as a stable interface for lithium metal anode

Jin Xie, Lei Liao, Yongji Gong, Yanbin Li, Feifei Shi, Allen Pei, Jie Sun, Rufan Zhang, Biao Kong, Ram Subbaraman, Jake Christensen, Yi Cui

Published 29 November 2017, *Sci. Adv.* **3**, eaao3170 (2017)
DOI: 10.1126/sciadv.aao3170

This PDF file includes:

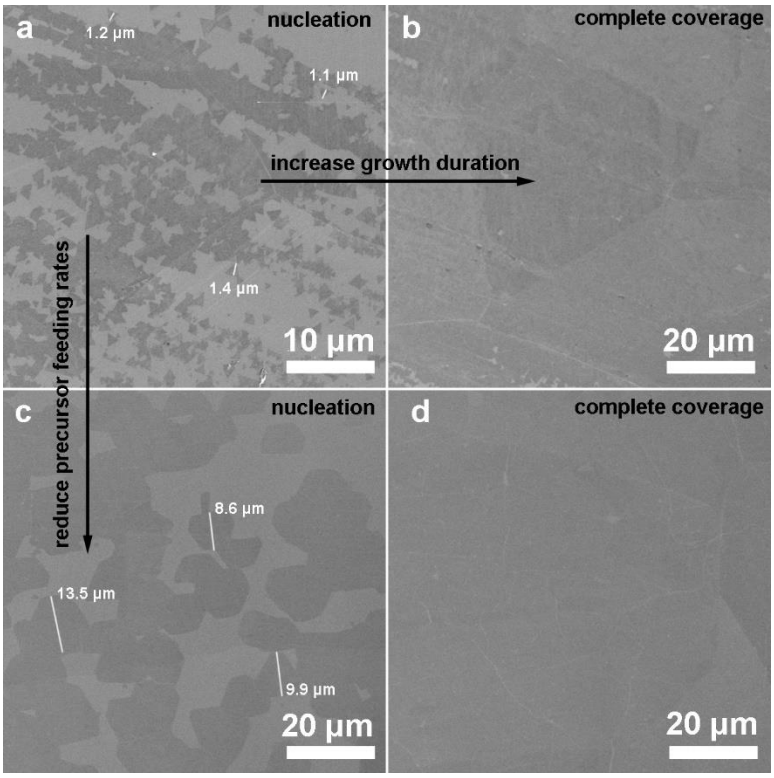

fig. S1. SEM characterization of CVD h-BN with different precursor feeding rates and growth durations on Cu substrates. (**a**) 90 °C precursor heating temperature and 15 minutes growth time; (**b**) 90 °C precursor heating temperature and 60 minutes growth time; (**c**) 70 °C precursor heating temperature and 30 minutes growth time; (**d**) 70 °C precursor heating temperature and 120 minutes growth time.

The morphology of h-BN films can be controlled by carefully adjusting precursor feeding rates and growth durations. Using ammonia borane (H_3N-BH_3) as the precursor, its feeding rate is a function of precursor heating temperature (*9, 10, 12-14*). At a low precursor heating temperature, the slow feeding of precursor lead to h-BN with low nucleation density but large domain sizes, or vice versa (fig. S1a and S1c). Continuous h-BN films covering the entire substrates can be obtained by extending the growth time (fig. S1b and S1d). For instance, at 90 °C precursor heating temperature, small-sized triangular shaped h-BN crystals can be obtained with 15 minutes growth duration (fig. S1a). For comparison, at 70 °C precursor heating temperature, continuous h-BN film with large domain sizes can be obtained with 120 minutes growth duration (fig. S1d). To

summarize, we obtained h-BN with relatively large grain sizes at low precursor heating temperature with extended growth time. However, the limitation for growing larger grain size defect free h-BN remains. First, the growth duration to grow large grain size h-BN is long because it requires slow growth rate. The overall process is time consuming for large-scale industrial production. Second, other defects, such as point defects originated from CVD process and cracks originated from transfer/processing, still exist. We believe our ALD process is a reliable alternative solution to solve the problems mentioned above.

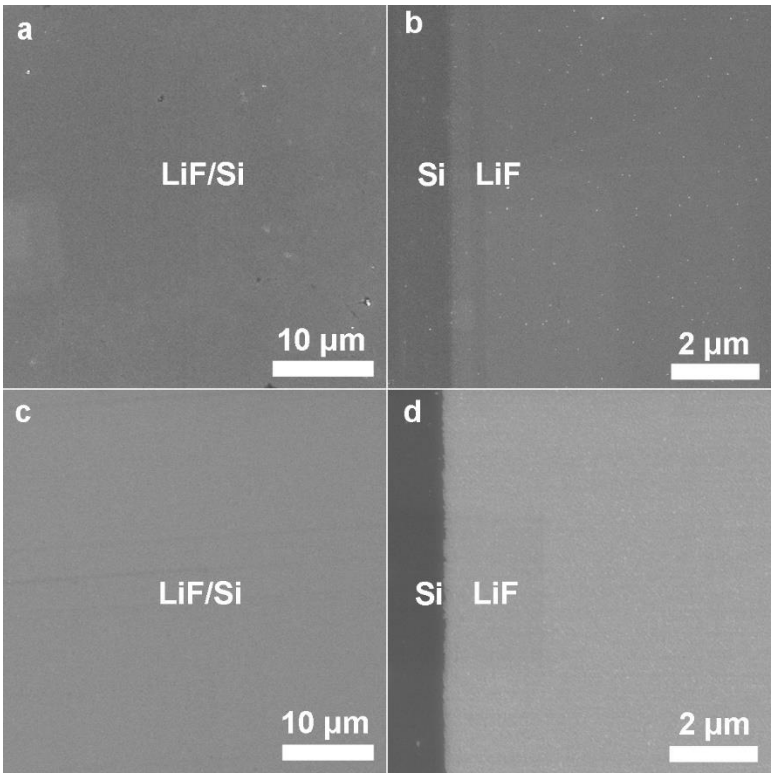

fig. S2. SEM characterization of ALD LiF on Si. (**a**, **b**) 50 ALD cycles of LiF deposition on Si; (**c**, **d**) 250 ALD cycles of LiF deposition on Si.

Atomic layer deposition of LiF in this study was carried out using lithium tert-butoxide (LiOtBu) and titanium fluoride (TiF_4) as precursors at a growth temperature of 250 °C. ALD is known for its ability to achieve a conformal coating. For instance, the ALD LiF film developed in this study was highly uniform on the pristine Si substrate (fig. S2a and S2b) with only 50 ALD cycles. In fig. S2b, the left-hand side of the Si wafer was protected by a high temperature resistant tape. After 50 ALD cycles of LiF deposition, the tape was removed to show the contrast between LiF deposition and no LiF deposition. SEM characterizations of 250 ALD cycles LiF deposition on Si were also given in fig. S2c and S2d.

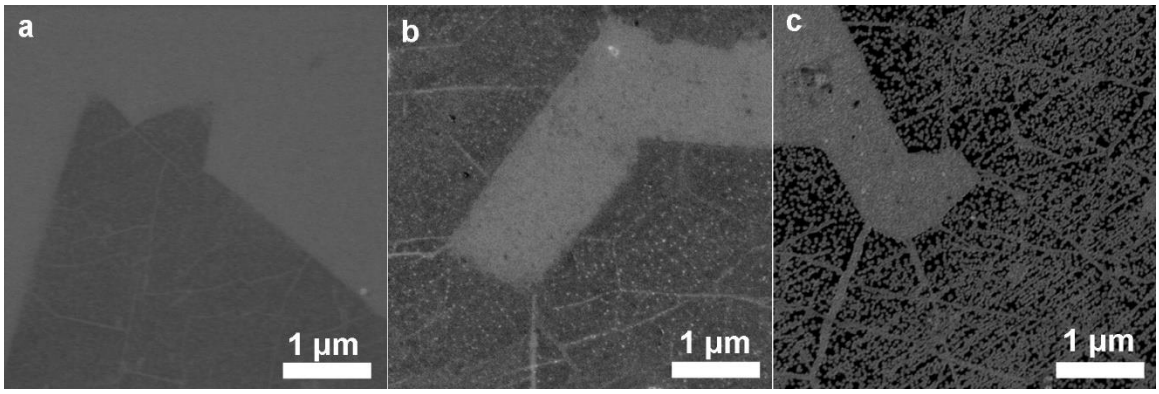

fig. S3. SEM characterization of ALD LiF on h-BN/Si. (**a**) 25 ALD cycles of LiF deposition on h-BN; (**b**) 50 ALD cycles of LiF deposition on h-BN; (**c**) 150 ALD cycles of LiF deposition on h-BN.

The amount of LiF deposition can be carefully controlled by varying ALD cycle numbers. Figure S3 shown 25 ALD cycles, 50 ALD cycles and 150 ALD cycles of LiF deposition on h-BN. While all samples shown selective LiF deposition, the diameters of LiF nanowires and the sizes of LiF nanoparticles increased with increasing ALD cycle numbers.

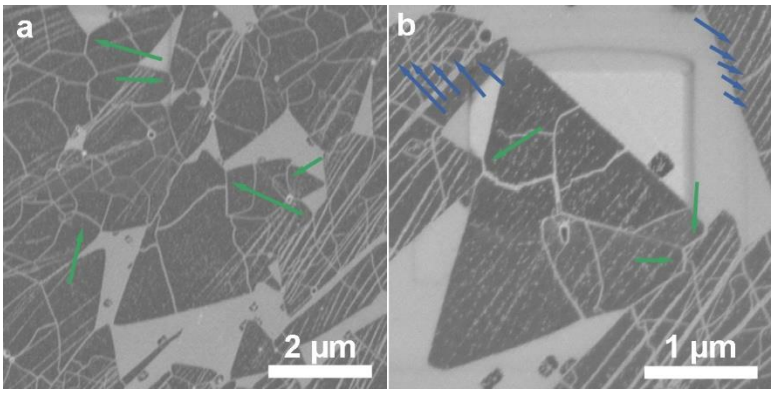

fig. S4. SEM characterization of ALD LiF on h-BN/Cu at different magnifications.

ALD LiF deposition on h-BN/Cu was characterized using SEM at different magnifications. It shared many similarities compared to ALD LiF deposition on h-BN/Si. Both nanowires and nanoparticles were observed after ALD LiF deposition on h-BN/Cu. However, they were two types of nanowires on LiF/h-BN/Cu (highlighted by green and blue arrows). One type of nanowires (highlighted by green arrows) locate on where two h-BN triangular domains meet, which is similar to what we have observed on LiF/h-BN/Si. This observation confirmed that the selective deposition on line defects does not depend on which type of substrates h-BN sit. In addition, our TEM study (see main text) also confirmed that the selective deposition is not substrate dependent as h-BN is suspended on hollow TEM grid. However, there is another type of nanowires (highlighted in blue arrows) observed on LiF/h-BN/Cu, which does not exist on LiF/h-BN/Si. Those nanowires are often parallel to each other, which suggested that the ALD LiF deposition might be also facilitated on Cu wrinkles induced by high temperature annealing of Cu (*52*).

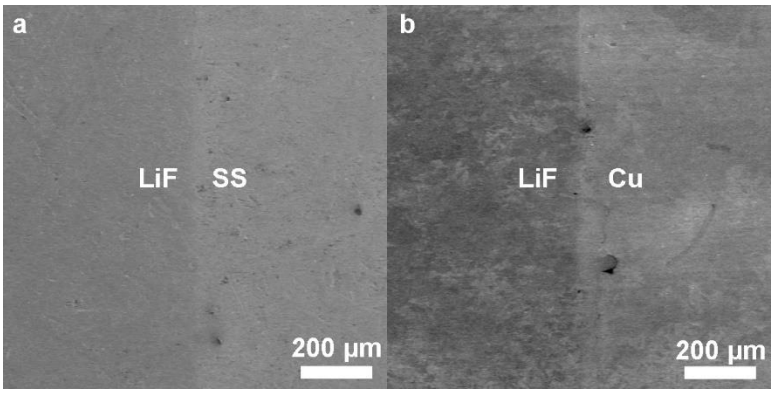

fig. S5. SEM characterization of ALD LiF on SS and Cu. SEM characterization of 50 ALD cycles of LiF deposition on a stainless steel (SS) spacer (**a**) and a piece of Cu current collector (**b**).

50 ALD cycles of LiF deposition was performed on both SS and Cu substrates with high uniformity across large areas. As shown in fig. S5, the right hand side of both substrates were protected by high temperature resistant tapes during deposition as a control to reveal pristine surfaces of SS and Cu (few tape residues were left on the right-hand side after the removal of the tape). Similar to ALD LiF deposition on the Si substrate, the left-hand side of SS was uniformly coated. The coverage of ALD LiF deposition on Cu was also uniform (the difference in contrast within the left-hand side was due to the orientation of different Cu grains).

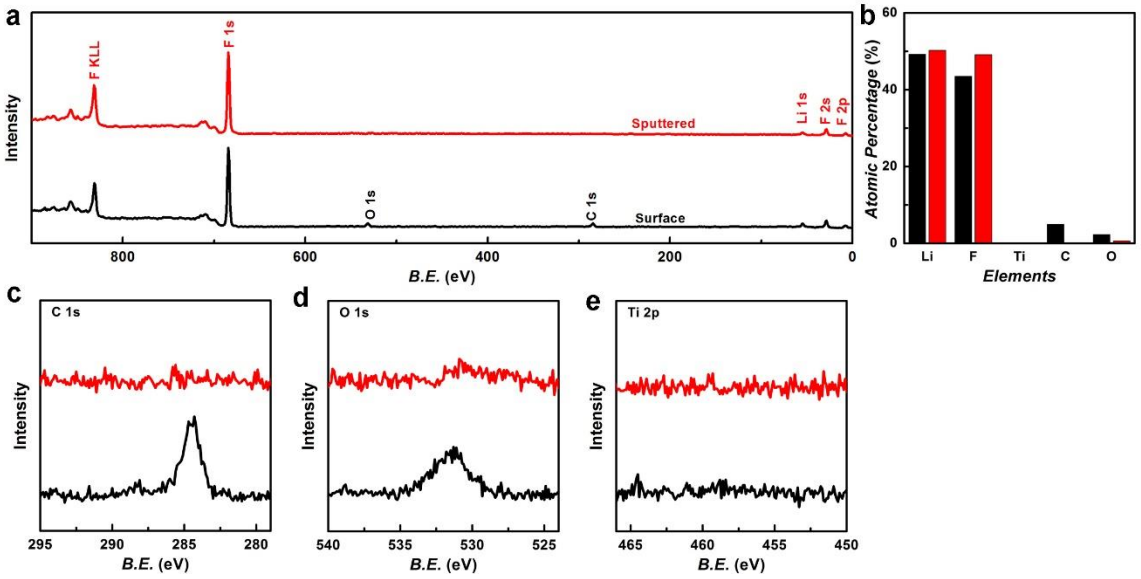

fig. S6. XPS analysis of ALD LiF on Si. (**a**) XPS characterization of an ALD LiF film on Si substrate with (red trace) and without (black trace) Ar sputtering; (**b**) chemical compositions of an ALD LiF film on Si substrate analyzed by XPS; (**c-e**) XPS fine scans of C 1s, O 1s, and Ti 2p peaks of an ALD LiF film on Si substrate.

XPS survey scans, fine scans and chemical composition analysis are presented in fig. S6 for an ALD LiF film grown on Si substrate before and after Ar sputtering. There were C and O impurities on the surface of the ALD LiF film before Ar sputtering; however, the intensities of C and O peaks were reduced after sputtering. The reduction of C and O peaks indicate that most of C and O signals come from surface absorbed species. The Li: F atomic ratio in the ALD LiF film after Ar sputtering was close to its stoichiometry value of 1 (Li: F = 1.02: 1), suggesting the good quality of LiF prepared by ALD. In survey scans and fine scans, no obvious Ti 2p peak has been identified. During the deposition, Ti could leave the surface of the film as $TiF_x(O^tBu)_y$ through ligand exchange reactions with another precursor, LiOtBu. Indeed, TiF_4 has been demonstrated as a reliable F precursor to produce various ALD metal fluoride films with little or no Ti residue (*53, 54*).

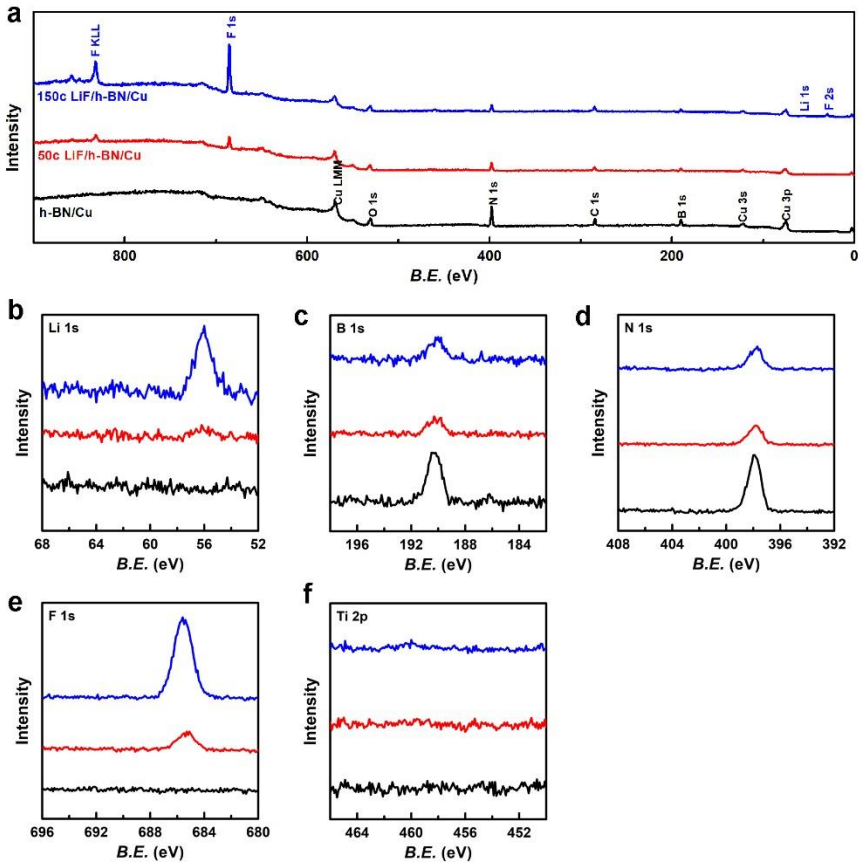

fig. S7. XPS analysis of ALD LiF on h-BN/Cu. (**a**) XPS characterization of h-BN/Cu, 50 ALD cycles of LiF on h-BN/Cu and 150 ALD cycles of LiF on h-BN/Cu electrodes; (**b-f**) XPS fine scans of Li 1s, B 1s, N 1s, F 1s, and Ti 2p peaks of h-BN/Cu, 50 ALD cycles of LiF on h-BN/Cu and 150 ALD cycles of LiF on h-BN/Cu electrodes.

XPS spectra of h-BN/Cu electrodes with different amount of ALD LiF deposition were compared in fig. S7. The pristine h-BN/Cu electrode showed B 1s peak and N 1s peak at 190.2 eV and 397.8 eV, both agreeing well with literature reports for h-BN (*6*, *7*). Upon ALD LiF coating, the intensities of Li 1s peak and F 1s peak increased with increasing LiF ALD cycle numbers. No Ti contamination has been observed.

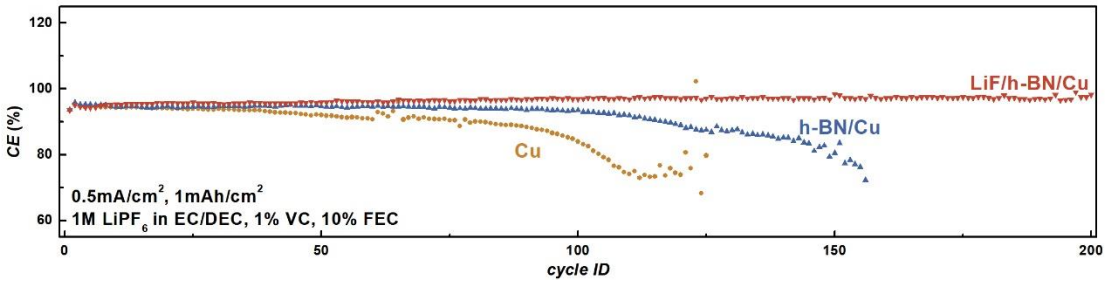

fig. S8. Cycling performance of Cu, h-BN/Cu, and LiF/h-BN/Cu electrodes in carbonate electrolyte with additives.

For Cu, h-BN/Cu and LiF/h-BN/Cu electrodes, their Coulombic efficiencies and cycle lives improved when additives (1% VC and 10% FEC) were added (fig. S8). Among them, the performance enhancement by adding additives was most obvious on pristine Cu electrode, presumably benefitted from a stronger SEI formed with the help of VC and FEC (*55*, *56*). On the contrary, the performance enhancement was least obvious on LiF/h-BN/Cu electrode when additives were added. The average Coulombic efficiency from 2nd cycle to 200th cycle of LiF/h-BN/Cu electrode was 96.6% in VC/FEC added electrolyte, presenting a small gain over additive free electrolyte. The result suggested that LiF/h-BN hybrid film itself is quite effective in preventing side reactions in between Li metal and carbonate electrolyte. Additives, such as VC/FEC, are effective on bare Cu electrolyte, but the enhancement from VC/FEC is less prominent when compared to the LiF/h-BN hybrid film in this case.

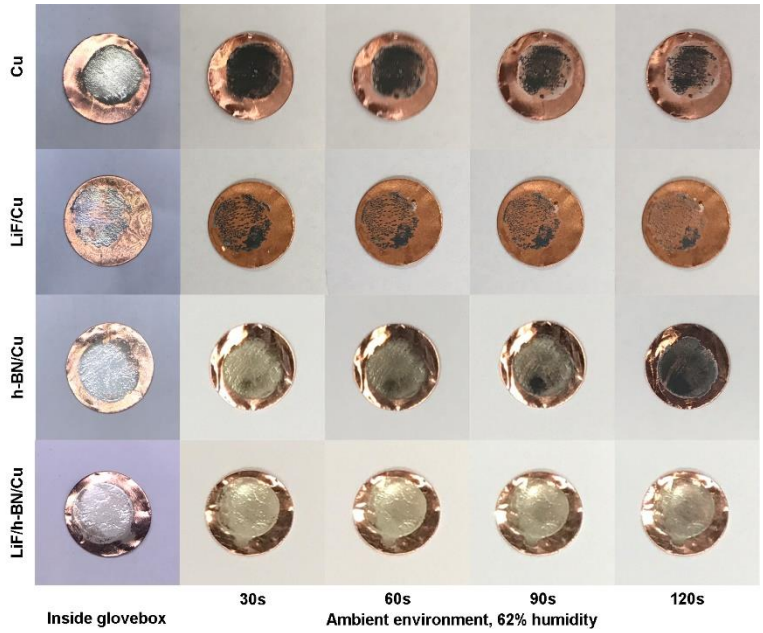

fig. S9. Optical images of Li-plated Cu, LiF/Cu, h-BN/Cu, and LiF/h-BN/Cu electrodes with different exposure times in the ambient environment. Optical images of Cu, LiF/Cu, h-BN/Cu and LiF/h-BN/Cu electrodes with electrochemically plated Li inside the glove box (left column) and in the ambient environment with a 62% humidity for different periods of times (right four columns: 30s, 60s, 90s and 120s).

Li metal is highly reactive and changes color when reacts with H_2O, CO_2 and N_2 in the ambient air. A perfect LiF/h-BN film coverage could in-principle prevent Li from reacting with air, and therefore keep Li metal's original metallic color. For example, Ajayan group has reported h-BN could prevent metal oxidation at high temperature by oxygen (*6*). As shown in fig. S9, all Li plated electrodes extracted from coin cells inside the glove box have shinny metallic color. The only difference is the Li plated on LiF/Cu electrode was not as uniform as Li plated on Cu, h-BN/Cu and LiF/h-BN/Cu. Such difference is in good agreement with SEM characterization in Fig. 4 of the main text. Electrodes were then taken out of the glove box and optical images were recorded at different time in the ambient environment (62% humidity at the time of measurement). The color of Li plated Cu electrode quickly changed from metallic color to black within 30s.

Similarly, the color of Li plated LiF/Cu electrode turned to black within 30s. The result suggested the native SEI is not effective in stopping Li degradation in the ambient environment. On the contrary, the color change was much slower for Li plated h-BN/Cu electrode, which turned to black in ~120s. The Li plated LiF/h-BN/Cu electrode was most resistant to ambient air attack, and its color change was least obvious within 120s. Such exceptional stability was attributed to the intact LiF/h-BN layer with Li plated underneath.

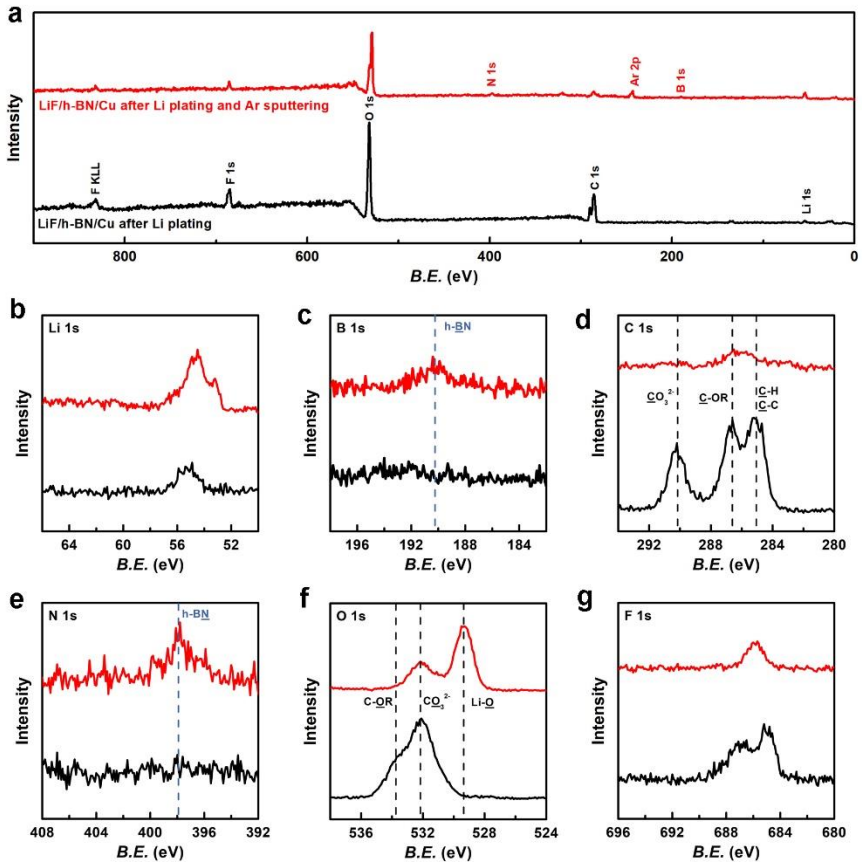

fig. S10. XPS analysis of the LiF/h-BN/Cu electrode after Li plating. (**a**) XPS characterization of LiF/h-BN/Cu electrode after Li plating with and without Ar sputtering; (**b**-**g**) XPS fine scans of Li 1s, B 1s, C 1s, N 1s, O 1s, and F 1s peaks of LiF/h-BN/Cu electrode after Li plating with and without Ar sputtering.

The LiF/h-BN/Cu electrode was extracted from the coin cell inside the glove box, rinsed by DEC, and then transferred into the XPS chamber directly via a sealed vessel to prevent exposure to the ambient environment. Shown in fig. S10, on LiF/h-BN/Cu after Li plating without Ar sputtering, electrolyte residual (e.g., $LiPF_6$) and SEI components (e.g., LiF, Li_2CO_3, LiCOOR) have been detected. The SEI layer formed by electrochemical reduction of carbonate electrolyte would cover the LiF/h-BN layer, and therefore no B 1s or N 1s peak could been detected on the surface. To further investigate the LiF/h-BN film, Ar sputtering was performed to remove electrolyte

residue and top SEI layer. After sputtering, B 1s peak and N 1s peak showed up at 190.3 eV and 397.7 eV. Both values were close to B 1s peak and N 1s peak in the pristine LiF/h-BN/Cu electrode, which suggested that h-BN is chemically stable upon Li plating. After Ar sputtering, Li 1s peak shifted to lower binding energy and no Cu signal has been detected, which indicated that the chemically stable LiF/h-BN hybrid film is in between the SEI layer and plated Li.

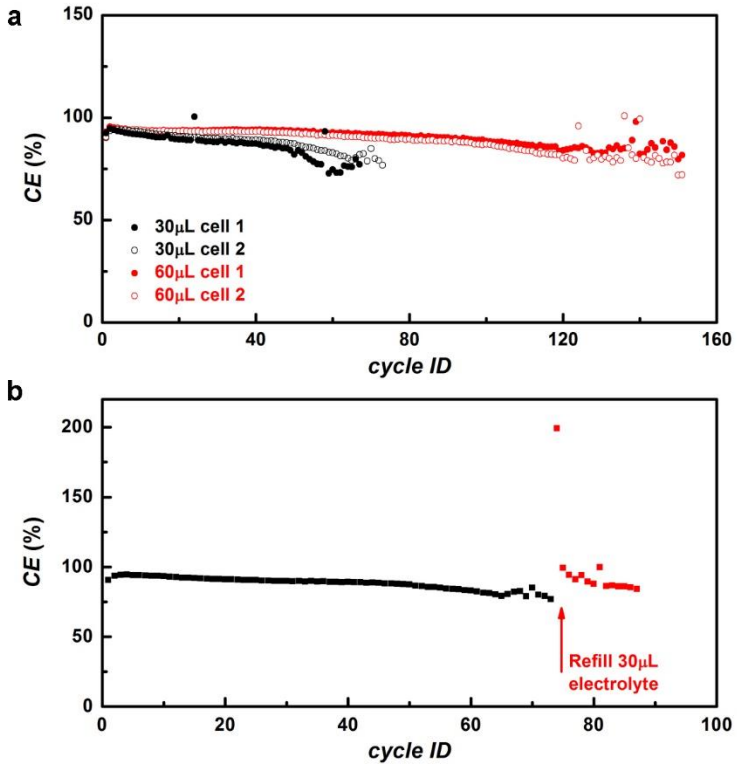

fig. S11. Cycling performance of batteries with different amounts of electrolyte and failed battery with refilled electrolyte. (**a**) Coulombic efficiency vs. cycle number plots of two batteries with 30 μL electrolyte and two batteries with 60 μL electrolyte; (**b**) Coulombic efficiency vs. cycle number of a failed battery with refilled electrolyte.

Several reasons may contribute to the battery failure including Li dendrite induced battery shorting, depletion of the active Li, depletion of the electrolyte, etc. Among them, battery shorting is the most dangerous, as it will lead to potentially severe safety events. Within the Li plating/stripping current density we explored in this study and with the help of double separators, we have not observed obvious battery shorting even using pristine Cu as the working electrode. Therefore, it allows us to use the Coulombic efficiency vs. cycle number as one key feature to monitor the status of battery. Nevertheless, preventing Li dendrite formation using stable interface is still important for future commercial applications in practical batteries where high rate

cycling and thin separators are desired to achieve both high power density and high energy density.

In this study, the main failure mode of the battery is the declining Coulombic efficiency over long cycles due to the side reactions between the Li and electrolyte. As the active Li is in excess from the Li counter electrode, we propose that the declining Coulombic efficiency is due to the consumption of the electrolyte. We found batteries with more added electrolyte could last longer than batteries with less added electrolyte (fig. S11a). With electrolyte being consumed by side reactions, the availability of Li transportation pathways are compromised and the Coulombic efficiency drop fast. We also found that once the Coulombic efficiency declined in the battery, we could restore the Coulombic efficiency by opening the coin cell and adding more electrolyte (other cell components including the working electrode and counter electrode are not changed) (fig. S11b). The Coulombic efficiency of the restored cell has an over 100% Coulombic efficiency during the 1st cycle, which is due to the dead Li accumulation during its previous failure cycles. After the 1st cycle, the average Coulombic efficiency of the restored cell is improved compared to the average Coulombic efficiency of the original cell. Therefore, it is important to improve the Coulombic efficiency, especially for practical cells, where both active Li and electrolyte are limited.